Supplementary Materials

for

A dual-trigger mode ionic hydrogel sensor for contact or contactless motions recognition

Qiao Wang, Hongyao Ding, Xiaosai Hu, Xiaoxu Liang, Miaomiao Wang, Qing Liu, Zongjin Li*, and Guoxing Sun*

Joint Key Laboratory of the Ministry of Education, Institute of Applied Physics and Materials Engineering, University of Macau, Avenida da Universidade, Taipa, Macau SAR, China.

Theoretical study of sandwich structure hydrogel with regular concavo-convex pattern

By modeling the regular concavo-convex pattern on the surface of P(AA-*co*-DMC), a larger capacitance of dielectric interlayer was formed caused by more contact area between P(AA-*co*-DMC) and P(AM-*co*-HEMAA) hydrogels. Importantly, compared with the conventional sandwich structure, the structured interface has advantages on the pressure sensitivity when samples are suffered the same external loads, including improving the friction between two layers and increasing the total deformation. As shown in **Fig. S1**, we separate a hexahedral differential element of sample to analyze the stress and strain. By applied the external vertically distributed loading, the body forces of the sample are expressed in **Equation S1 (** ρ is the density of hydrogel (≈1kg/m^3)**,** g=9.8N/kg**)**. In this loading condition, we assume that the sensor only deforms along the z axis, as defined in **Equation S2**, where *u, v, w* are the deformation along the *x, y, z* axis, respectively.

$$f_x = 0,\ f_y = 0, f_z = \rho g \tag{S1}$$

$$u = 0, v = 0, w = w(z) \tag{S2}$$

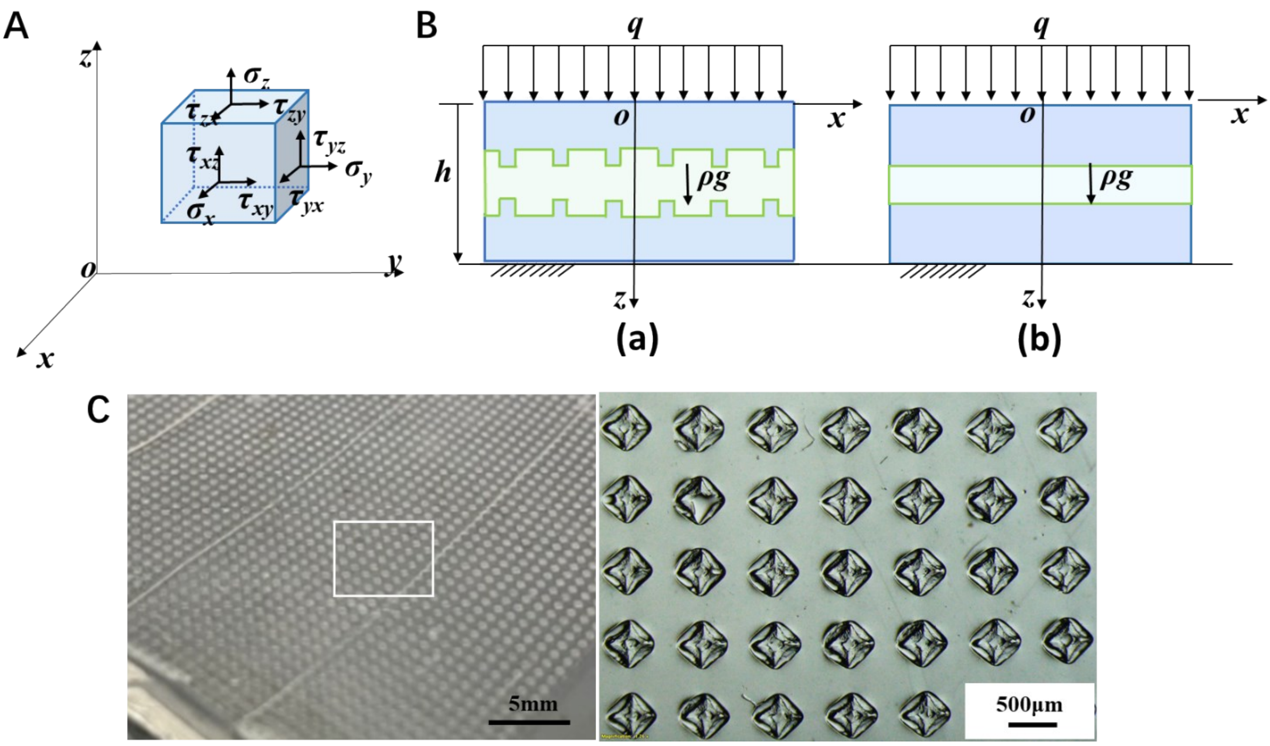

Figure S1. Theoretical analysis on the effect of regular concavo-convex pattern in sandwich structure. (**A**) Stress analysis of hexahedral differential element in hydrogel-based sensor. (**B**) Illustration of the sandwich structure with or without regular concavo-convex pattern at interface which suffers the external load. (**a**) Illustration of MOMS structure section. (**b**) Illustration of comment sandwich structure section. (**C**) The morphology of regular concavo-convex pattern on the surface of P(AA-*co*-DMC) hydrogel.

The relationship between stress and strain components along three axes can be expressed in **Equation S3**, where $\sigma_x, \sigma_y, \sigma_z$ are the components of the normal stress, $\tau_{yz}, \tau_{zx}, \tau_{xy}$ are the components of the shear stress, $\varepsilon_x, \varepsilon_y, \varepsilon_z$ are the components of the normal strain, $\gamma_{yz}, \gamma_{zx}, \gamma_{xy}$ are the shearing strains, E is the elastic modulus, μ is Poisson's ratio of hydrogel ($\mu \approx 0.46$[1]). Meanwhile, **Equation S4** shows the correlation of the strains and displacements. Then, the relationship between stress and deformation (**Equation S5**) can be derived by substituting the **Equation S4** into **Equation S3.**

$$\left.\begin{aligned}
\varepsilon_x &= \frac{1}{E}[\,\sigma_x - \mu(\sigma_y + \sigma_z)] \\
\varepsilon_y &= \frac{1}{E}[\,\sigma_y - \mu(\sigma_x + \sigma_z)] \\
\varepsilon_z &= \frac{1}{E}[\,\sigma_z - \mu(\sigma_x + \sigma_y)] \\
\gamma_{yz} &= \frac{2(1+\mu)}{E}\tau_{yz} \\
\gamma_{zx} &= \frac{2(1+\mu)}{E}\tau_{zx} \\
\gamma_{xy} &= \frac{2(1+\mu)}{E}\tau_{xy}
\end{aligned}\right\} \tag{S3}$$

$$\left.\begin{aligned}
&\varepsilon_x = \frac{\partial u}{\partial x}, \varepsilon_y = \frac{\partial v}{\partial y}, \varepsilon_z = \frac{\partial w}{\partial z} \\
&\gamma_{yz} = \frac{\partial w}{\partial y} + \frac{\partial v}{\partial z}, \gamma_{zx} = \frac{\partial u}{\partial z} + \frac{\partial w}{\partial x}, \\
&\gamma_{xy} = \frac{\partial v}{\partial x} + \frac{\partial u}{\partial y}
\end{aligned}\right\} \tag{S4}$$

$$\left.\begin{aligned}
\sigma_x &= \frac{E}{1+\mu}\left(\frac{\mu}{1-2\mu}\theta + \frac{\partial u}{\partial x}\right), \\
\sigma_y &= \frac{E}{1+\mu}\left(\frac{\mu}{1-2\mu}\theta + \frac{\partial v}{\partial y}\right), \\
\sigma_z &= \frac{E}{1+\mu}\left(\frac{\mu}{1-2\mu}\theta + \frac{\partial w}{\partial z}\right), \\
\tau_{yz} &= \frac{E}{2(1+\mu)}\left(\frac{\partial w}{\partial y} + \frac{\partial v}{\partial z}\right), \\
\tau_{zx} &= \frac{E}{2(1+\mu)}\left(\frac{\partial u}{\partial z} + \frac{\partial w}{\partial x}\right), \\
\tau_{xy} &= \frac{E}{2(1+\mu)}\left(\frac{\partial v}{\partial z} + \frac{\partial u}{\partial y}\right),
\end{aligned}\right\} \tag{S5}$$

and $\theta = \frac{\partial u}{\partial x} + \frac{\partial v}{\partial y} + \frac{\partial w}{\partial z} = \frac{\partial w}{\partial z}$.

By incorporation of the **Equation S5** and differential equations of mechanics equilibrium theory, **Equation S6** can be further established. Subsequently, according to the boundary conditions including $(-\sigma_z)_{z=0} = q \ and \ (w)_{z=h} = 0$, we could get the total deformation along the vertical section (Δ), as shown in **Equation S7** and **S8**. Compared with the comment sandwich structure, due to the difference of *E* between different material layers, the Δ value of MOMS is larger under the same loading condition, thereby generating more intense capacitive variation and achieving better sensitivity.

$$\left.\begin{aligned}\frac{E}{2(1+\mu)}\left(\frac{1}{1-2\mu}\frac{\partial\theta}{\partial x}+\nabla^2 u\right)+f_x=0,\\ \frac{E}{2(1+\mu)}\left(\frac{1}{1-2\mu}\frac{\partial\theta}{\partial y}+\nabla^2 v\right)+f_y=0,\\ \frac{E}{2(1+\mu)}\left(\frac{1}{1-2\mu}\frac{\partial\theta}{\partial z}+\nabla^2 w\right)+f_z=0,\end{aligned}\right\} \tag{S6}$$

and $$\nabla^2=\frac{\partial^2}{\partial x^2}+\frac{\partial^2}{\partial y^2}+\frac{\partial^2}{\partial z^2},\ \frac{\partial\theta}{\partial x}=0,\frac{\partial\theta}{\partial y}=0,\frac{\partial\theta}{\partial z}=\frac{d^2w}{dz^2}.$$

$$w=\frac{(1+\mu)(1-2\mu)}{E(1-\mu)}\left[q(h-z)+\frac{\rho g}{2}(h^2-z^2)\right] \tag{S7}$$

$$\Delta=\int_z (w)\,dz \tag{S8}$$

The characterization and mechanical properties of the P(AA-*co*-DMC) hydrogel and P(AM-*co*-HEMAA)

The zwitterionic hydrogel exhibited the typical porous three-dimensional network, which has advantage on the transport of the mobile ions (**Fig. S2**A). As shown in **Fig. S2**B, the FTIR spectrum of PAA hydrogel exhibited characteristic peaks at 3345, 1550, 1450, and 1405 cm^{-1} corresponded to -OH stretching, C=O stretching of -COONa, and C=O deformation vibration of -COOH, respectively. By contrast, the spectrum of PDMC had five main characteristic absorption bands including the peaks at 1713, 1643, 1485, 1299, and 960 cm^{-1} corresponded to C-O γ absorption band, C=C γ absorption band, $(CH_2)_2$ δ absorption band, quaternary ammonium $N^+(CH_3)_3$ absorption band, and C-O δ absorption band. All these characteristic absorption bands were performed in the P(AA-co-DMC) hydrogel spectrum, which determined the copolymer had a DMC and AA block structure.

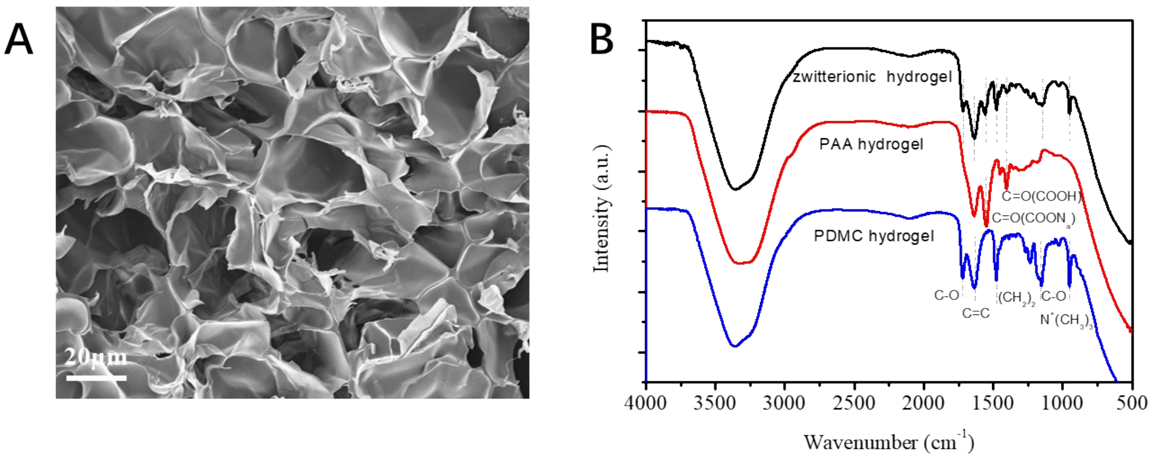

Figure S2. The morphology and composition analysis of P(AA-*co*-DMC) hydrogel (mole ratio=1). (**A**) The typical SEM images of the freeze-dried xerogels for the zwitterionic hydrogel. (**B**) The composition analysis of polyacrylic acid (PAA), Polymethyl propylene oxyethyl trimethylammonium chloride (PDMC), and P(AA-*co*-DMC) hydrogel.

As for the electric conductivity of the zwitterionic hydrogel and P(AM-co-HEMAA) hydrogel synthesized in this work, the resistance of the sample with a size of 10*8*1.03 mm^3 is 4.33 Ω and 64.2 Ω, respectively. Based on the following equation, the conductivity of P(AA-co-DMC) hydrogel and P(AM-co-HEMAA) hydrogel are equal to 2.97 S/m and 0.20 S/m, respectively .

$$\sigma = \frac{1}{R_b} \cdot \frac{d}{S} \tag{S9}$$

Where σ is the conductivity of the sample, R_b is the resistance, d is the thickness, and S is the effective area.

Moreover, we further tested the dielectric property of the P(AM-co-HEMAA) hydrogel. It performs the satisfying permittivity under the frequency with a range of 200 kHz-20 MHz, which is a guarantee for the sensing performance of this kind of capacitive hydrogel system.

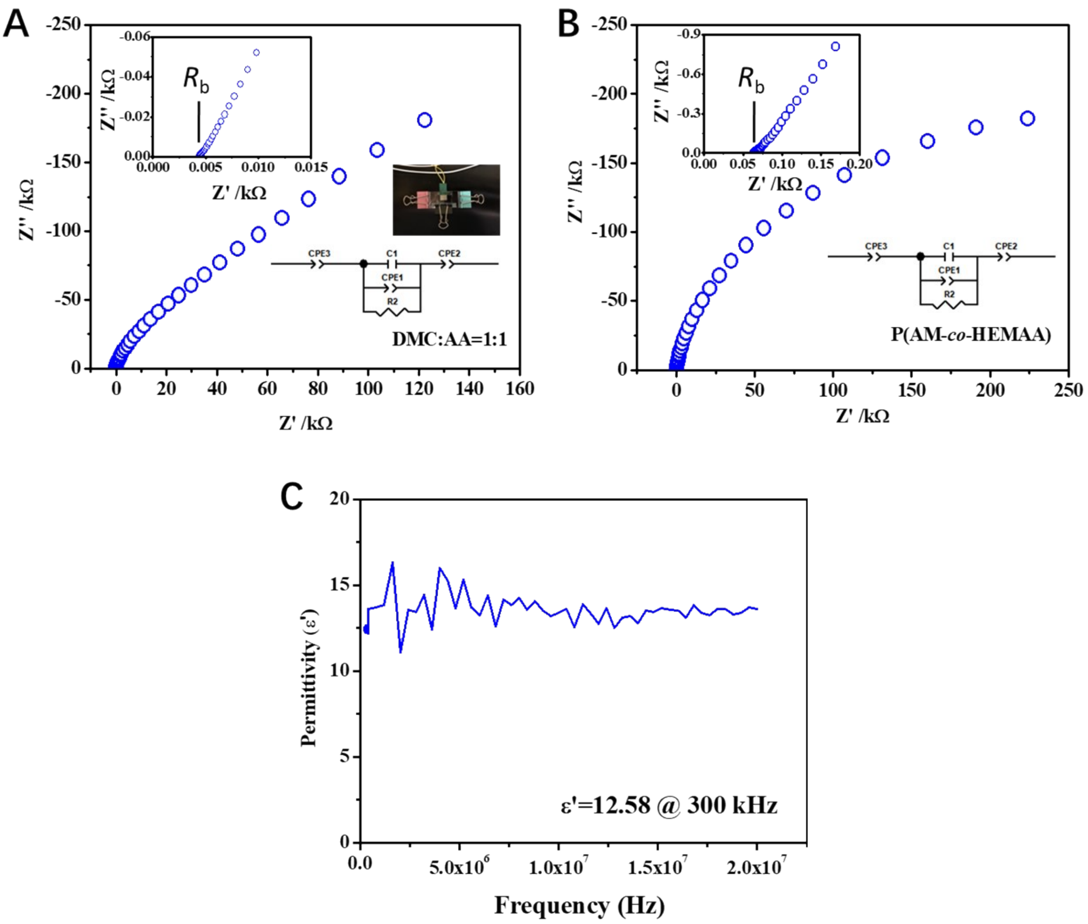

Figure S3. Electrochemical Impedance Spectroscopy of the hydrogels with 5 mV amplitude and 0.01-10^5 Hz frequency. (**A**) Electrochemical Impedance Spectroscopy of the P(AA-*co*-DMC) hydrogel (mole ratio=1). The upper left image inset is the enlargement, and the bottom right is the equivalent circuit. (**B**) Electrochemical Impedance Spectroscopy of the P(AM-*co*-HEMAA) hydrogels. The upper left image inset is the enlargement, and the bottom right is the equivalent circuit. (**C**) The permittivity of P(AM-co-HEMAA) hydrogel from 200 kHz to 20 MHz.

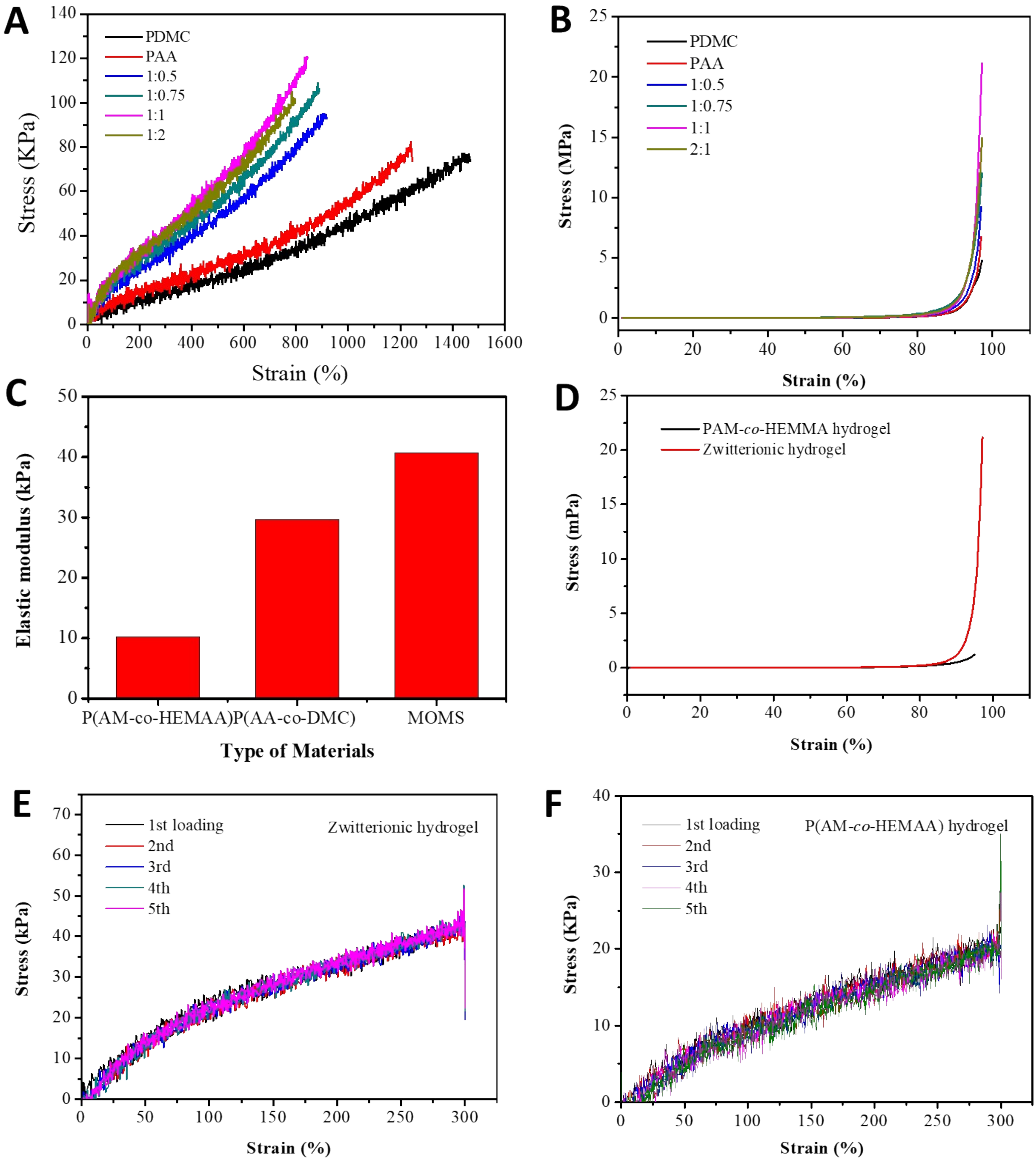

Figure S4. Mechanical Properties of P(AA-*co*-DMC) hydrogels with different proportion and components of MOMS. (**A, B**) Tension and compression tests for (AA-*co*-DMC) hydrogels with different mole ratio at room temperature. (**C**) Comparation of each components and MOMS elastic modulus. (**D**) The compression tests for P(AA-co-DMC) and P(AM-co-HEMAA) hydrogel. (**E,F**) Cyclic elongation tests for P(AA-*co*-DMC) and P(AM-*co*-HEMAA) hydrogel at 3-fold tensile strain.

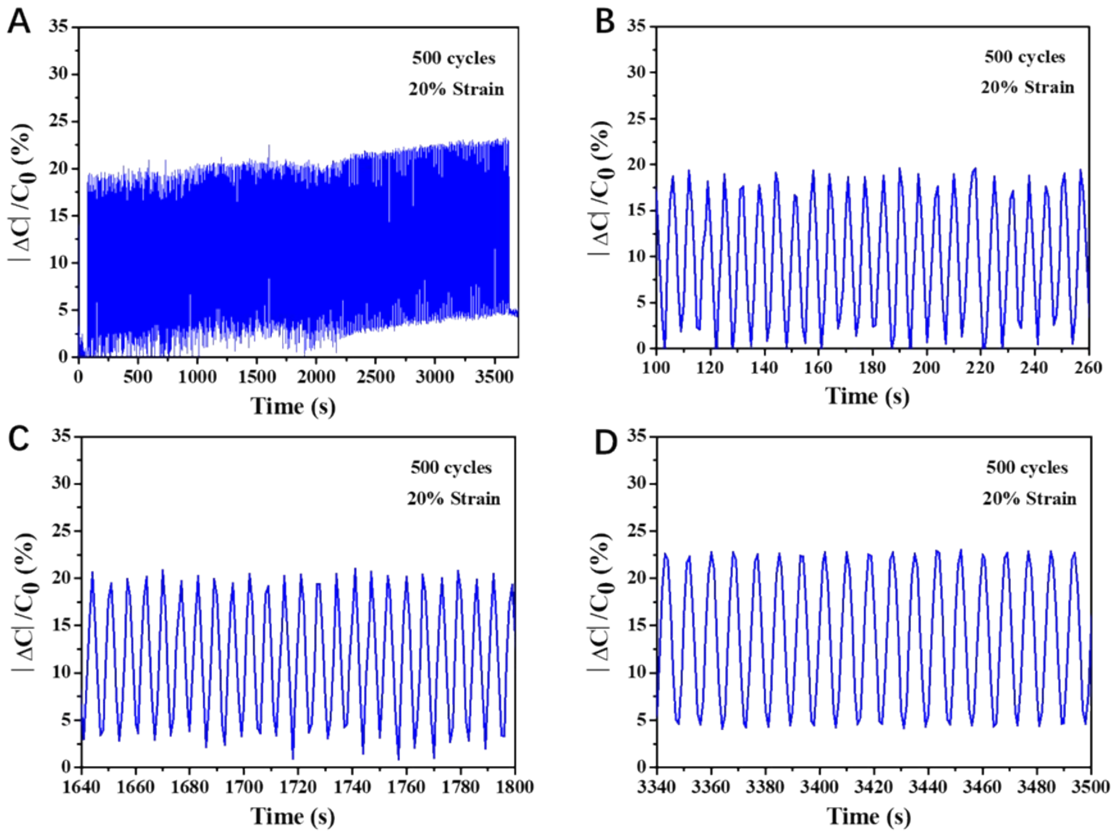

Figure S5. The stability and durability of MOMS suffering cyclic loading. (A)The 500 cyclic tension experiment with 20% elongation under the speed of 10 mm/s. (B, C, D) The enlargement of the figure A during 100-260 s, 1640-1800 s, and 3340-3500 s sections.

Theoretical analysis of the capacitance changes of MOMS in touch-free mode

Based on the **Equation 1 & 2**, the capacitance variations generated by the changes of distance and effective overlap area between finger and MOMS surface can be got in the **Equation S10**. Therefore, by detecting the variation values, the recognition of diverse noncontact gestures and monitor on hands remote motions can be achieved accurately. As a result, the more satisfying and freedom human–machine interfaces experience for screen sensors, wearable devices, intelligent robots, and home automation will be achieved.

$$\frac{\Delta C}{C_0} = \frac{C_{EDL} + C_D}{C_{EDL} + 2C_D}\left(\frac{1}{C_{finger}\frac{C_{EDL} + C_D}{C_D C_{EDL}} + 1} - 1\right), \tag{S10}$$

and $$C_{finger} = \frac{\varepsilon S_{finger}}{4\pi k' d_{finger}}.$$

Where C_{EDL} is the capacitance of the EDL, C_D is the capacitance of the dielectric hydrogel, C_{finger} is the capacitance formed between finger and electrolyte hydrogel, ε is the dielectric constant of the dielectric layer, *S* is the effective area of the conducting layer, k' is the electrostatic constant, and *d* is the thickness of the dielectric.

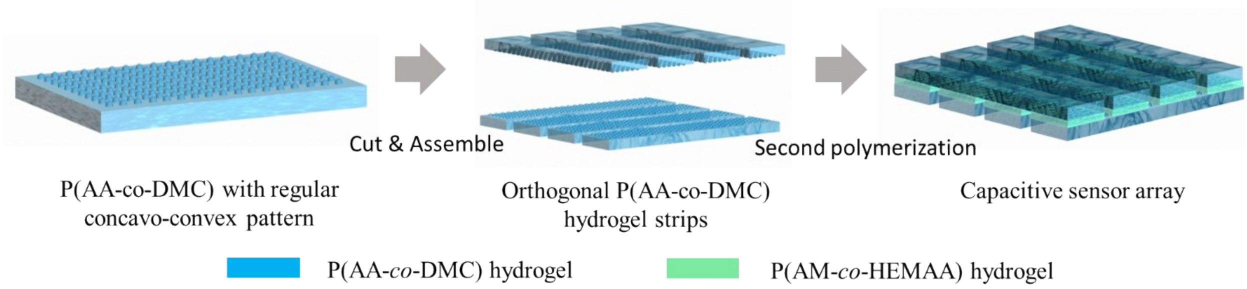

Figure S6. The schematics of fabrication process of a 4 × 4 array sensors with two-step method.

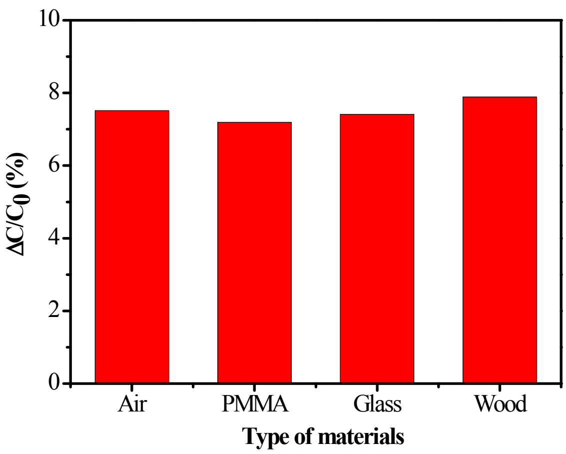

Figure S7. Capacitance variation signals of the sensor with various cover materials (2 mm thickness) to a palm at the same working distance (3 mm).

Monomer	Chemical structure
Acroleic acid (AA)	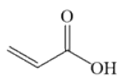
[2-(Methacryloyloxy)ethyl] trimethylammonium chloride (DMC)	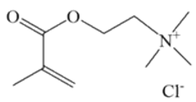
Acrylamide (AM)	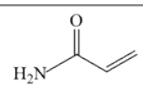
N-(2-Hydroxyethyl)acrylamide (HEMAA)	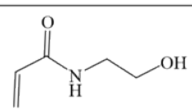

Table S1. The chemical structure of monomers used in this work

Movie S1

The performance on wrist pulse detection.

Movie S2

The performance on the remote gesture movements detection of MOMS.

Movie S3

The performance on the remote gesture movements detection of MOMS covered by different materials.

Reference

[S1] U. Chippada, B. Yurke, N. A. Langrana. Simultaneous determination of Young's modulus, shear modulus, and Poisson's ratio of soft hydrogels. Journal of Materials Research, 2010, 25, 3, 545-555.